A mutation in *Rab27a* causes the vesicle transport defects observed in *ashen* mice

Scott M. Wilson*, Richard Yip*, Deborah A. Swing*, T. Norene O'Sullivan*, Yuke Zhang†, Edward K. Novak†, Richard T. Swank†, Liane B. Russell‡, Neal G. Copeland*, and Nancy A. Jenkins*§

*Mouse Cancer Genetics Program, National Cancer Institute–Frederick Cancer Research and Development Center, Frederick, MD 21702; †Department of Molecular and Cell Biology, Roswell Park Cancer Institute, Buffalo, NY 14263; and ‡Biology Division, Oak Ridge National Laboratory, Oak Ridge, TN 37831

Contributed by Liane B. Russell, May 11, 2000

The *dilute* (*d*), *leaden* (*ln*), and *ashen* (*ash*) mutations provide a unique model system for studying vesicle transport in mammals. All three mutations produce a lightened coat color because of defects in pigment granule transport. In addition, all three mutations are suppressed by the semidominant *dilute-suppressor* (*dsu*), providing genetic evidence that these mutations function in the same or overlapping transport pathways. Previous studies showed that *d* encodes a major vesicle transport motor, myosin-VA, which is mutated in Griscelli syndrome patients. Here, using positional cloning and bacterial artificial chromosome rescue, we show that *ash* encodes *Rab27a*. Rab GTPases represent the largest branch of the p21 Ras superfamily and are recognized as key players in vesicular transport and organelle dynamics in eukaryotic cells. We also show that *ash* mice have platelet defects resulting in increased bleeding times and a reduction in the number of platelet dense granules. These defects have not been reported for *d* and *ln* mice. Collectively, our studies identify *Rab27a* as a critical gene for organelle-specific protein trafficking in melanocytes and platelets and suggest that *Rab27a* functions in both MyoVa dependent and independent pathways.

More than 50 loci in the mouse have been identified that affect pigmentation of the coat (1). Three of these loci (*d*, *ln*, and *ash*) have been grouped together because they have an identical phenotype: Pigment granule (melanosome) synthesis is normal in these mice, but melanosome transport is abnormal (2). In wild-type mice, melanins are synthesized in melanosomes, specialized organelles derived from the Golgi. The melanosomes are then transported along the dendrites and exported to neighboring keratinocytes in the hair bulb and subsequently to the hair shaft (2, 3). In mice homozygous for these three recessive mutations, the melanosomes are localized mainly in the perinuclear region of the melanocyte (3–5) resulting in the uneven release of pigment into the hair bulb and a lightened coat color.

Genetic evidence suggests that these loci encode proteins that function in the same or overlapping pathway. For example, mice homozygous for any double, or the triple, combinations of *d*, *ln*, and *ash* on the *nonagouti* background all have the same phenotype as mice homozygous for any of the individual mutations (N.G.C. and N.A.J., unpublished observations). In addition, all three mutations are suppressed by the semidominant suppressor, *dsu* (6, 7). *dsu* was first recognized by its ability to suppress the coat color phenotype of *d* mice and in subsequent experiments was also shown to partially suppress the coat color phenotype of *ash* and *ln* mice (6). In all cases, the level of suppression could be correlated with the extent of the restoration of normal melanosome distribution. *dsu* has no phenotype on its own, is cell autonomous (8), and can be seen only in combination with *d*, *ash*, or *ln*.

In addition to the melanosome transport defect, *d* null mice also show a neurological defect, characterized by opisthotonus and ataxia, which results in the death of the animal 2–3 weeks after birth. The neurological defect is thought to result from the failure to transport smooth endoplasmic reticulum (SER) from the dendritic shaft to the dendritic spines of cerebellar Purkinje cells (9, 10). The absence of SER in spines probably disrupts the regulation of intracellular Ca^{2+} and postsynaptic signal transduction.

A retroviral integration into the *d* gene in mice carrying the *dilute-viral* (d^v) allele allowed the cloning of the *d* gene and the demonstration that *d* encodes an unconventional myosin heavy-chain, myosin Va (MyoVa) (11, 12). MyoVa is expressed at high levels in nearly all tissues in the adult (12) and has the expected structure for a member of this family—i.e., a globular head domain containing the ATP- and actin-binding sites, a "neck" domain, which is the site of calmodulin (or light-chain) binding, and a tail domain, which is thought to represent the cargo-binding domain. MyoVa acts as a dimer and moves along actin filaments in a plus-end-directed manner (13). Human MYOVA mutations have also been identified and shown to produce Griscelli syndrome, a rare autosomal recessive disorder characterized by pigment dilution, variable cellular immunodeficiency, neurological defects, and acute phases of uncontrolled lymphocyte and macrophage activation (14).

Yeast two-hybrid studies have shown that the tail domain of MyoVa can interact with a microtubule-based transport motor, ubiquitous kinesin heavy chain (KhcU) (15). Considerable biological and biochemical evidence indicates that long-range transport in animal cells occurs on microtubules, whereas short-range transport occurs on actin filaments (16). An important question raised by these studies is how transport along these pathways is coordinated. The yeast two-hybrid studies suggest that one way this transport is coordinated is through the direct interaction of the different motor molecules. These data are consistent with previous studies, which showed that MyoVa and kinesin both can bind synaptic vesicles in the rat (17, 18) and that MyoVa is required for short-range, but not long-range, transport of smooth endoplasmic reticulum in Purkinje cells (9, 10).

MyoVa has also been shown to bind to a novel RING finger protein BERP (19). It thus appears that MyoVa transports cargo as part of a complex involving several different proteins including KhcU and BERP. An intriguing possibility is that *ash* and *ln* also encode proteins that function as part of this motor complex. To determine whether this is the case, we have initiated the positional cloning of *ash* and *ln*. In studies described here, we present evidence to show that *ash* encodes *Rab27a*. Rab proteins are recognized as key players in vesicular transport and organelle dynamics in eukaryotic cells.

Abbreviations: MyoVa, myosin-VA; YAC, yeast artificial chromosome; SSLP, simple sequence length polymorphism; BAC, bacterial artificial chromosome; HPS, Hermansky Pudlak syndrome; CHM, choroideremia.

Data deposition: The sequence reported in this paper has been deposited in the GenBank database (accession no. bankit332438).

§To whom reprint requests should be addressed. E-mail: jenkins@ncifcrf.gov.

The publication costs of this article were defrayed in part by page charge payment. This article must therefore be hereby marked "*advertisement*" in accordance with 18 U.S.C. §1734 solely to indicate this fact.

Article published online before print: *Proc. Natl. Acad. Sci. USA*, 10.1073/pnas.140212797. Article and publication date are at www.pnas.org/cgi/doi/10.1073/pnas.140212797

Methods

Mice. C3H/HeSn-*ash*/*ash* and *Mus castaneus* (CAST/Ei) mice were purchased from The Jackson Laboratory and maintained and propagated at the National Cancer Institute–Frederick Cancer Research and Development Center, Frederick, MD. Mice carrying the *d-se* deficiency chromosomes 13SaSd, 11FHAFo, 19Zb, 1DTD, 9R250M, 37FBFo, 17Zb, and 10FDFoD were obtained from the Oak Ridge National Laboratory, Oak Ridge, TN.

Genetic and Physical Maps. Genetic and yeast artificial chromosome (YAC)-based physical maps of the *ash* critical region were generated as described (20). A 129/Sv bacterial artificial chromosome (BAC) library (Research Genetics, Huntsville, AL) was screened with the simple sequence length polymorphism (SSLP) markers and YAC end probes derived from the *ash* critical region. Positive BACs were end sequenced by using SP6 and T7 promoter primers. PCR primer pairs, designed from the BAC end sequence, were then used to construct a BAC contig of the *ash* critical region.

Deficiency Mapping. To further refine the *ash* critical region, eight deficiency chromosomes (21, 22) were tested for their ability to complement *ash* by crossing mice carrying the deficiencies with C3H/HeSn-*ash*/*ash* mice. Three deficiency chromosomes (13SaSd, 11FHAFo, 19Zb) complemented *ash* function, and the remaining five deficiency chromosomes (1DTD, 9R250M, 37FBFo, 17Zb, 10FDFoD) did not. Next, each deficiency chromosome was balanced over a *Mus castaneus* chromosome, and DNA from these mice was then analyzed for the presence or absence of molecular markers that cosegregated with *ash* in backcross mice (*D9Mit340, 64F2R, D9Mit166, D9Mit341*). The order of the molecular markers in relation to the deficiency breakpoints and *ash* was: centromere-(9R250M, 37FBFo, 17Zb, 10FDFoD)-*D9Mit340*-1DTD-(*ash*, 64F2R, *D9Mit166*)-19Zb-*D9Mit341*-(13SaSd, 11FHFAFo).

BAC Complementation. Individual BAC DNAs were isolated and injected into C3H/HeSn-*ash*/*ash* zygotes as described (23). Transgenic mice were identified by Southern blot analysis of genomic DNA isolated from tail biopsies (24) and by coat color. Founder animals were backcrossed to homozygous *ash* mice and their progeny scored for the presence of the BAC transgene and the *ash* coat color phenotype.

Cloning of *Rab27a* cDNA. A mouse *Rab27a* probe was generated by reverse transcription–PCR by using primers designed from the rat sequence (nucleotides 2–25 and 449-426) (25). The mouse probe was subsequently used to screen a Stratagene mouse melanocyte cDNA library. The largest cDNA isolated extended from nucleotide −185 to +1827.

RNA Isolation and Reverse Transcription–PCR. Total mouse RNA was isolated from 3- to 4-week-old animals by using STAT-60 RNAzol (Tel-Test, Friendswood, TX). Poly(A) RNA was purified by using an Ambion Poly(A) Pure isolation kit (Ambion, Austin, TX). cDNA was synthesized from both poly(A) and total RNA by using the GIBCO/BRL SUPERSCRIPT Preamplification System (GIBCO/BRL). These cDNAs were then amplified by using mouse *Rab27a*-specific primers (nucleotides 259–280 and 449–426) or *microphthalmia transcription factor* (*Mitf*)-specific primers (nucleotides 296–319 and 605–582) as a control. After 40 cycles of PCR, the reactions were analyzed on a 3% TAE Metaphor gel (FMC).

Mutation Detection. Genomic DNAs from both the mutant and wild-type strain of origin were amplified by using *Rab27a* primers, which flank the fourth intron (nucleotides 259–280 and 449–426). PCR products were gel purified by using a GeneClean III kit (BIO 101, Vista, CA) and then subjected to direct DNA sequencing. In addition, aberrantly spliced *Rab27a* transcripts from the mutant strain were cloned and subjected to DNA sequencing. Sequencing was performed by using the Big Dye Terminator Cycle Sequencing Ready Reaction Kit (Perkin–Elmer), and data were acquired on an ABI Model 377 DNA sequencer (Applied Biosystems).

Hematology. Bleeding times were determined by tail bleeding as described (26). Platelets were lysed in 1 ml distilled water and assayed fluorimetrically for serotonin (27). Platelet-rich plasma was collected from citrated undiluted blood by centrifugation at $150 \times g$ for 10 min as described (26). Unfixed and unstained platelets were rapidly air dried on carbon-coated grids before electron microscopy (28).

Melanocyte Cell Culture. Melanocyte cell lines were isolated from skin of mutant and wild-type mice as described (29).

Results and Discussion

A Genetic and Physical Map of the *ash*-Critical Region. To initiate the positional cloning of *ash*, we generated 897 (C3H/HeSn-*ash*/*ash* × *Mus castaneus*) × C3H/HeSn-*ash*/*ash* N_2 progeny, which were typed at weaning for *ash* by visual inspection. Tail DNAs from the mice were then typed for SSLP markers predicted to map near *ash*, defining an *ash*-critical interval of ≈0.3 cM or about 600 kb (Fig. 1*a*). Coincident with these studies, we also performed deficiency mapping. *ash* resides in the *dilute* (*d*)-*short-ear* (*se*) complex of mouse chromosome 9, which is defined by complementation analysis of overlapping deletions (21). Eight deficiency chromosomes, three that complemented *ash* (13SaSd, 11FHAFo, 19Zb) and five that did not (1DTD, 9R250M, 37FBFo, 17Zb, 10FDFoD), were balanced over *M. castaneus* chromosomes and analyzed for the presence or absence of markers used in the mapping cross. The results indicated that *ash* resides between the breakpoints of the 19Zb and 1DTD deficiencies (Fig. 1*b*). Next, we established a physical map of the interval. SSLP markers from the *ash*-critical interval were used to identify and characterize four YACs from the region (Fig. 1*b*). Subsequently, the SSLPs and other markers developed from the YACs were used to establish a BAC contig for the region (Fig. 1*b*).

Identification of an *ash* Candidate Gene. During the development of the *ash* physical map, YAC-end sequencing showed that the left-end sequence of YAC 165E4 contained a portion of the coding region of *Rab27a* (25, 30). Rab proteins form the largest branch of the Ras superfamily of small GTPases (31). They are localized to the cytoplasmic face of organelles, and vesicles involved in the biosynthetic/secretory and endocytic pathways in eukaryotic cells and have been shown to play an essential role in the processes that underlie the targeting and fusion of transport vesicles with their appropriate acceptor membranes. *Rab27a* was thus an excellent candidate for *ash*. To test this candidate gene, we isolated a full-length 1.3-kb *Rab27a* cDNA from a wild-type mouse melanocyte library. Genomic sequence analysis showed that the putative 221-aa Rab27a protein is encoded by five exons, similar to the human *RAB27A* gene (32). These exons are not altered in the 19Zb-deficiency chromosome but are completely deleted in the 1DTD deficiency, consistent with the hypothesis that *ash* encodes *Rab27a* (Fig. 1*b*).

***Rab27a* Expression Is Altered in *ash* Mice.** Reverse transcription–PCR analysis of *Rab27a* expression in wild-type and *ash* tissues provided additional evidence that *ash* encodes *Rab27a*. Although a single *Rab27a* transcript was identified in all wild-type

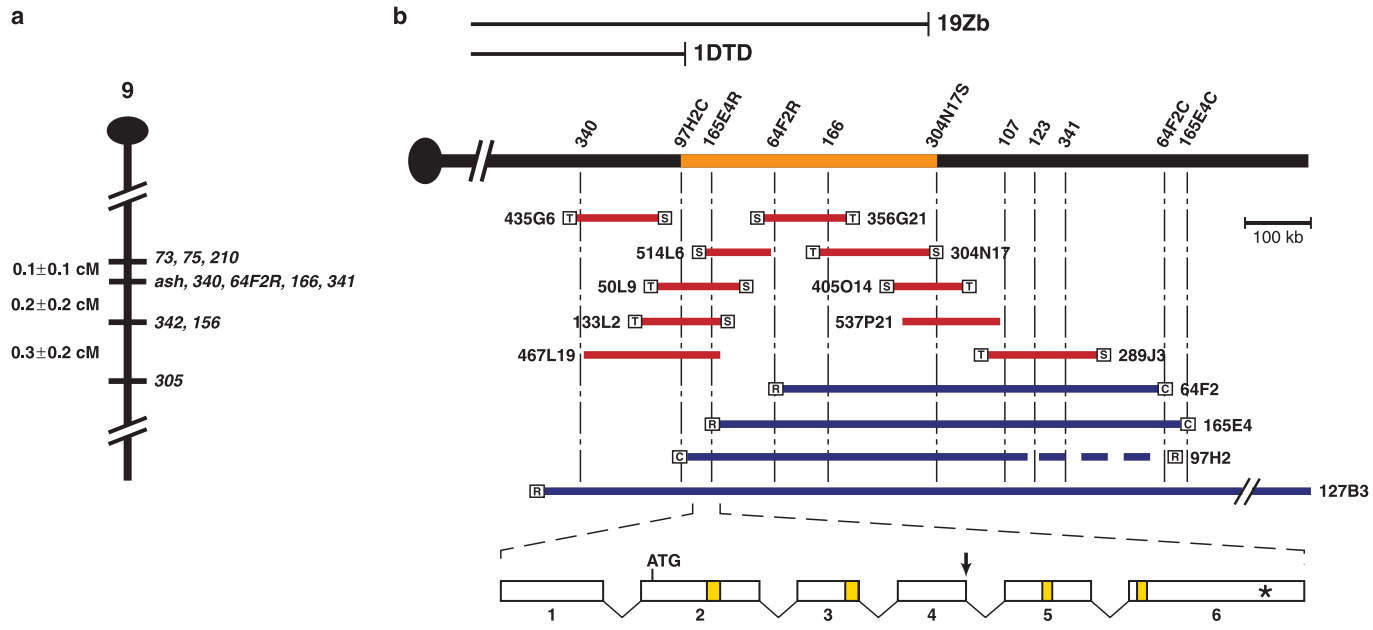

Fig. 1. Meiotic and physical linkage maps of the *ash*-critical region. (*a*) A meiotic linkage map showing the positions of SSLP markers (*D9Mit* followed by a number) that map within or near the *ash*-critical region. The centromere is at the top (filled circle). Marker 64F2R is from the *URA3* end of YAC 64F2. (*b*) The positions of several molecular markers are shown on the chromosome at the top, as are the position of two deficiency breakpoints (19Zb and 1DTD). BACs in red (S, Sp6 end; T, T7 end), drawn to scale, and YACs in blue (R, *URA3* end; C, yeast centromere end), not drawn to scale, are shown below the chromosome. The *URA3* end of YAC 97H2 was chimeric as indicated by the dashed line. The *ash*-critical region is drawn in orange. The intron and exon structure of *Rab27a* is shown at the bottom with the yellow boxes representing sequences that are part of the GTP-binding pocket; the arrowhead indicates the site of the *ash* mutation, and the * represents the location of the poly(A) addition site

tissues analyzed, a larger-sized abnormal transcript was detected in tissues homozygous for *ash* (Fig. 2*a*). These results indicated that *ash* might be caused by an insertion or splicing defect in the *Rab27a* gene.

A Splice Site Mutation in *Rab27a* in *ash* Mice. Consistent with these results, sequence analysis of the *Rab27a* coding region from wild-type C3H/HeSn (the strain of origin of the *ash* mutation) (33) and *ash* mice identified a single A-to-T transversion in the

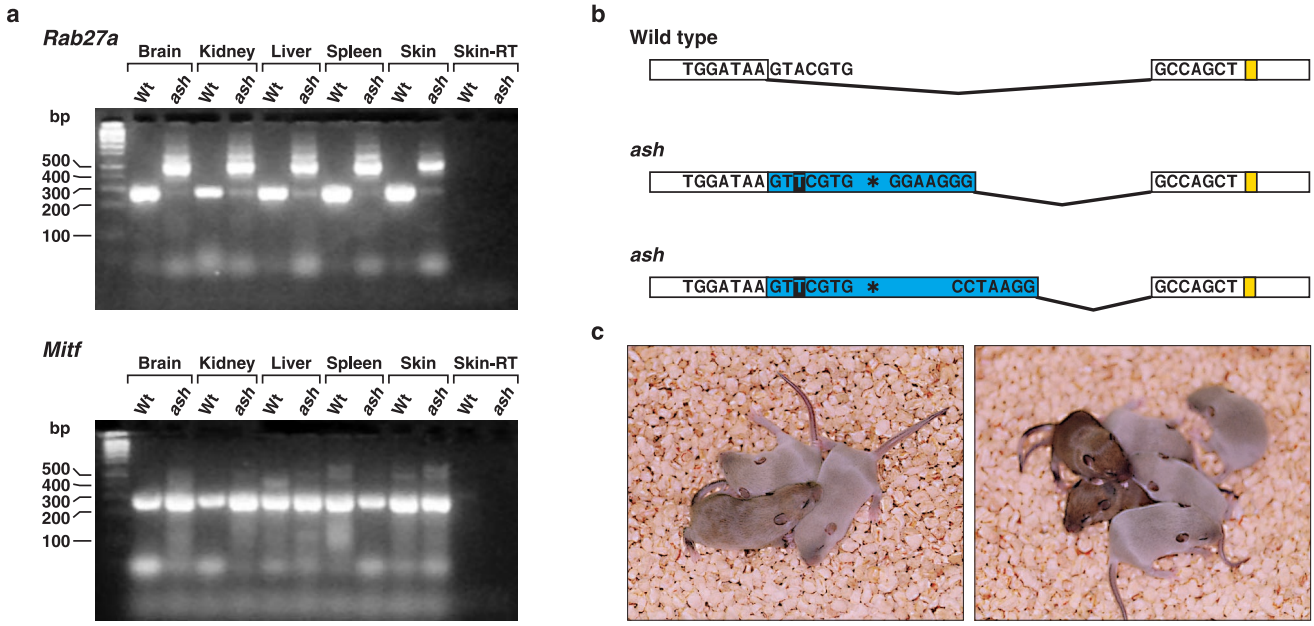

Fig. 2. The *ash* mutation results from a defect in *Rab27a*. (*a*) Reverse transcription–PCR analysis of *Rab27a* expression in wild-type and homozygous *ash* mice. *Mitf* was amplified as a control. Note that *ash* mice express a mutant *Rab27a* transcript that is not expressed in wild-type mice. Sequence analysis indicates that this mutant transcript is actually composed of two transcripts, which contain 235 or 252 bp of intron sequence, respectively. Skin-RT, minus reverse transcriptase control. (*b*) A mutation in the exon 4 splice donor site of *Rab27a* in *ash* mice. Exons 4 and 5 are indicated by open rectangles, whereas intron sequences are shown in blue. Exon 5 sequences contributing to the GTP-binding pocket are shown in yellow. The location of the A-to-T transversion in the exon 4 splice donor site (black box) and the stop codon in intron sequence (star) are also indicated. (*c*) BAC rescue of *ash*. A partially rescued BAC 514L6 animal is shown on the left, whereas two completely rescued BAC 133L2 animals are shown on the right.

third base pair of the splice donor site located downstream of exon 4 (Figs. 1*b* and 2*b*). The mutation leads to the activation of two cryptic downstream splice donor sites, resulting in the incorporation of 235 or 252 bp of intron sequence into the *Rab27a* message. These two mutant transcripts are presumably nonfunctional because there is an in-frame stop codon in the intron sequence, which would lead to the production of truncated proteins lacking two critical domains of the GTP-binding pocket. Although mutational studies have defined the function of a number of Rab proteins in lower eukaryotes, to our knowledge this is the first example of a Rab mutation in mammals.

Wild-type *Rab27a* transcripts are also expressed at low levels in *ash* mice (Fig. 2*a*). However, because two (now extinct) remutations to *ash* have been identified that are phenotypically identical to the C3H/HeSn *ash* allele (34) (N.G.C. and N.A.J., unpublished results), it appears that these wild-type transcripts are not sufficient to rescue what is likely to be the null phenotype at the locus.

BAC Rescue. To confirm that *Rab27a* encodes *ash*, we performed BAC rescue. BACs 514L6 and 133L2 overlap by ≈50 kb and carry *Rab27a* in this common region (Fig. 1*b*). The two BACs were injected into homozygous *ash* embryos and the progeny examined at weaning for coat color and for the presence of the BAC. Six BAC 514L6-positive animals were obtained and five showed partial rescue (Fig. 2*c Left*). Eight BAC 133L2-positive animals were obtained, and five showed complete rescue (Fig. 2*c Right*), whereas two showed partial rescue (data not shown). These results indicate that both BACs carry the *ash* gene and provide confirmation that *Rab27a* encodes *ash*. At present, we do not know why BAC 514L6 preferentially generates partially rescued animals, although it is important to note that all progeny generated from these partially rescued founders showed complete rescue.

Platelet Granule Defects in *ash* Mice. In addition to pigment defects, *ash* mice have defects in platelet dense granules. Wet-mount electron microscopic examination of platelets from mutant and control mice identified 1.3 +/− 0.2 dense granules per platelet in *ash* mice vs. 8.4 +/− 0.5 in C3H controls after looking at >80 platelets ($P < 0.001$) (Fig. 3). Similar disparities were found for dense granule constituents such as serotonin (0.2 +/− 0.04 $\mu g/10^9$ platelets in *ash* mice vs. 2.8 +/− 0.2 $\mu g/10^9$ platelets in C3H controls). As expected, these platelet defects lead to increased bleeding times for *ash* mice (>15 min for *ash* vs. 1.7 min. for C3H controls; $P < 0.001$). These results place Rab27a within a melanocyte/platelet subfamily of Rab proteins and are consistent with sequence and expression data, which also indicate that Rab27a and its close relative Rab27b belong to a melanocyte/platelet subfamily of Rab proteins (30).

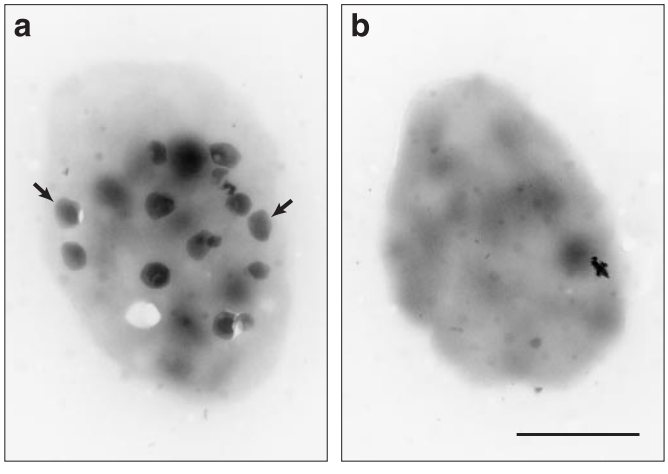

Fig. 3. Electron micrographs showing platelet defects in *ash* mice. Electron micrographs of instantaneously air-dried and unstained whole platelets from (*a*) normal C3H/HeSn and (*b*) homozygous C3H/HeSn-*ash* mice. Arrows indicate typical dense granules of a normal platelet. Bar = 1 μm.

***ash* Mice Are a Good Hermansky Pudlak Syndrome (HPS) Model.** *ash* mice have similar organelle defects as those observed in HPS patients (35). HPS is a rare autosomal recessive disorder characterized by oculocutaneous albinism and platelet storage pool deficiency. Over time, some HPS patients also develop pulmonary fibrosis and granulomatous colitis, presumably because of accumulation of undegraded materials in lysosomes of reticuloendothelial cells. All of the organelles affected in HPS patients (and *ash* mice) maintain acidic interiors and are therefore considered to be biogenetically related to lysosomes (3, 36). Two genes have been identified that are mutated in HPS patients, a 79-kDa protein of unknown function and the β3A subunit of the AP-3 adaptor complex (37, 38). Interestingly, mutant strains of mice have been identified that carry mutations in both HPS genes [*pale ear* (*ep*) and *pearl* (*pe*)] (39–41), establishing a correspondence between the human and mouse multiorganellar pigmentation mutants. In view of these results, a screen for *RAB27A* mutations in HPS patients would now seem warranted.

Loss of *RAB27A* Function Is Not the Ultimate Cause of Choroideremia (CHM). RAB27A is unique among the RABs in that it is selectively unprenylated in cells from patients with CHM, an X-linked retinal disorder that results from defects in REP1, the enzyme that attaches geranylgeranyl groups to the C terminus of Rab proteins (42). The traffic-directing function of Rab proteins depends on their binding to cell membranes, and this in turn depends on a 20-carbon geranylgeranyl isoprene unit, which is attached in thioether linkage to cysteine residues near the C terminus of the protein. RAB27A is also expressed in two retinal cell layers that degenerate earliest in CHM patients. This has lead to speculation that loss of RAB27A function is the ultimate cause of CHM (43). Our studies, however, do not support this hypothesis. Although retinal defects have been reported in *Rep1* knockout mice, the retinas of *ash* mice appear normal.

***ash* Melanocytes Have Normal Dendritic Arbors.** Originally, the lightened coat color of *d*, *ln*, and *ash* mice was thought to result from a defect in melanocyte morphology. *In vivo*, it appeared that melanocytes from these strains lacked the extensive dendritic arbor through which these cells normally deliver their pigment-laden granules to keratinocytes (Fig. 4*a*). The absence of this dendritic arbor was thought to cause the melanosomes to be unevenly released into the hair bulb keratinocytes. *In vitro* studies, however, showed that *d* and *ln* melanocytes have normal dendritic arbors and suggested that these mutations result from melanosome transport defects (44, 45) (e.g., see Fig. 4*b*). To determine whether this were also true for *ash*, we cultured melanocytes from neonatal C3H/HeSn-*ash*/*ash* skin. As shown in Fig. 4*c*, *ash* melanocytes also have normal dendritic arbors.

***Rab27a* Function in Melanocytes.** Visualization of melanosome dynamics within wild-type and *d* melanocytes indicates that long-range melanosome transport occurs on microtubules and is MyoVa independent (46). MyoVa-dependent interactions of melanosomes with F-actin occur in the periphery where they prevent melanosomes from returning on microtubules to the cell center. We do not yet know whether Rab27a is required for the microtubule-dependent movement of melanosomes, although the phenotypic similarity of *d* and *ash* melanocytes (compare Fig. 4 *b* and *c*), including the presence of a limited number of melanosomes within the dendritic arbor of *ash* melanocytes, is

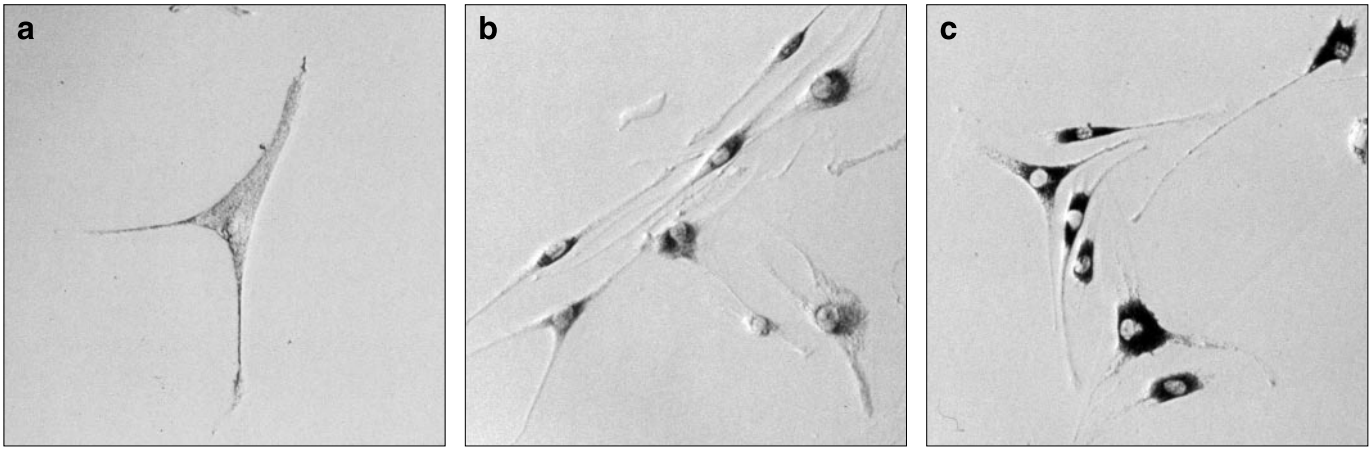

Fig. 4. Cultured melanocytes from *ash* mice have normal dendritic arbors. Melanocyte cell lines were established from neonatal skin of wild-type (*a*), *dilute* (*b*), and *ashen* (*c*) mice. Note that the melanosomes clump in the perinuclear region of *dilute* and *ashen* melanocytes even though they have normal dendritic arbors.

consistent with the hypothesis that Rab27a functions in the periphery, perhaps in concert with MyoVa. Support for this hypothesis has come from studies in yeast. Conditional mutants of *sec4* (analogous to mammalian *Rab*) and *myo2*, a yeast homologue of MyoVa, show similar defects in secretion and accumulation of post-Golgi vesicles and fail to complete budding under nonpermissive conditions (47, 48). *myo2 sec4* double mutants are, however, synthetically lethal (49), providing genetic evidence that these genes function in the same transport pathway.

MyoVa-Independent Functions of Rab27a. The platelet defects we observed in *ash* mice have not been reported for *d* or *ln* mice. This result suggests that Rab27a also functions in MyoVa-independent pathways. Because these mutations all affect the coat, they are particularly amenable to enhancer/suppressor screens involving *N*-ethyl-*N*′-nitrosourea mutagenesis, which could ultimately lead to the identification of other members of these different pathways.

Rab27a/MyoVa Complexes? A kinesin-like protein, termed Rabkinesin-6, has recently been identified that interacts with the GTP-bound forms of Rab6 (50). Rabkinesin-6 localizes to the Golgi apparatus and plays a role in the dynamics of this organelle. The carboxyl-terminal domain of Rabkinesin-6, which contains the Rab6-interacting domain, inhibits the effects of Rab6-GTP on intracellular transport, establishing Rabkinesin-6 as a potential effector of Rab6 function. These studies support the hypothesis that Rab proteins (or at least some of them) act in concert with molecular motors to regulate directional membrane transport and dynamics of intracellular organelles. In future studies, it will be important to determine whether MyoVa functions as part of a complex with Rab27a.

This research was supported by the National Cancer Institute, the Department of Health and Human Services (N.G.C. and N.A.J.), National Institutes of Health grants EY12104 and HL31698 (R.T.S.), Roswell Park Cancer Institute Cancer Support grant CA16056, and the U. S. Department of Energy at the Oak Ridge National Laboratory, managed by University of Tennessee-Batelle, Limited Liability Company, contract DE-AC05–00OR22725 (L.B.R.). In addition, we thank Madonna Reddington for excellent technical assistance.

1. Jackson, I. J. (1991) *BioEssays* **13,** 439–446.
2. Silvers, W. K. (1979) in *The Coat Colors of Mice* (Springer, New York).
3. Orlow, S. J. (1995) *J. Invest. Dermatol.* **105,** 3–7.
4. Provance, D. W., Jr., Wei, M., Ipe, V. & Mercer, J. A. (1996) *Proc. Natl. Acad. Sci. USA* **93,** 14554–14558.
5. Wu, X., Bowers, B., Wei, Q., Kocher, B. & Hammer, J. A., 3rd (1997) *J. Cell. Sci.* **110,** 847–859.
6. Moore, K. J., Swing, D. A., Rinchik, E. M., Mucenski, M. L., Buchberg, A. M., Copeland, N. G. & Jenkins, N. A. (1988) *Genetics* **119,** 933–941.
7. Moore, K. J., Seperack, P. K., Strobel, M. C., Swing, D. A., Copeland, N. G. & Jenkins, N. A. (1988) *Proc. Natl. Acad. Sci. USA* **85,** 8131–8135.
8. Moore, K. J., Swing, D. A., Copeland, N. G. & Jenkins, N. A. (1994) *Genetics* **138,** 491–497.
9. Dekker-Ohno, K., Hayasaka, S., Takagishi, Y., Oda, S., Wakasugi, N., Mikoshiba, K., Inouye, M. & Yamamura, H. (1996) *Brain Res.* **714,** 226–230.
10. Takagishi, Y., Oda, S., Hayasaka, S., Dekker-Ohno, K., Shikata, T., Inouye, M. & Yamamura, H. (1996) *Neurosci. Lett.* **215,** 169–172.
11. Jenkins, N. A., Copeland, N. G., Taylor, B. A. & Lee, B. K. (1981) *Nature (London)* **293,** 370–374.
12. Mercer, J. A., Seperack, P. K., Strobel, M. C., Copeland, N. G. & Jenkins, N. A. (1991) *Nature (London)* **349,** 709–713.
13. Mermall, V., Post, P. L. & Mooseker, M. S. (1998) *Science* **279,** 527–533.
14. Pastural, E., Barrat, F. J., Dufourcq-Lagelouse, R., Certain, S., Sanal, O., Jabado, N., Seger, R., Griscelli, C., Fischer, A. & de Saint Basile, G. (1997) *Nat. Genet* **16,** 289–292.
15. Huang, J. D., Brady, S. T., Richards, B. W., Stenolen, D., Resau, J. H., Copeland, N. G. & Jenkins, N. A. (1999) *Nature (London)* **397,** 267–270.
16. Langford, G. M. (1995) *Curr. Opin. Cell Biol.* **7,** 82–88.
17. Leopold, P. L., McDowall, A. W., Pfister, K. K., Bloom, G. S. & Brady, S. T. (1992) *Cell Motil. Cytoskeleton* **23,** 19–33.
18. Prekeris, R. & Terrian, D. M. (1997) *J. Cell Biol.* **137,** 1589–1601.
19. El-Husseini, A. E. & Vincent, S. R. (1999) *J. Biol. Chem.* **274,** 19771–19777.
20. Fletcher, C. F., Lutz, C. M., O'Sullivan, T. N., Shaughnessy, J. D., Jr., Hawkes, R., Frankel, W. N., Copeland, N. G. & Jenkins, N. A. (1996) *Cell* **87,** 607–617.
21. Russell, L. B. (1971) *Mutat. Res.* **11,** 107–123.
22. Rinchik, E. M., Russell, L. B., Copeland, N. G. & Jenkins, N. A. (1986) *Genetics* **112,** 321–342.
23. Antoch, M. P., Song, E. J., Chang, A. M., Vitaterna, M. H., Zhao, Y., Wilsbacher, L. D., Sangoram, A. M., King, D. P., Pinto, L. H. & Takahashi, J. S. (1997) *Cell* **89,** 655–667.
24. Jenkins, N. A., Copeland, N. G., Taylor, B. A. & Lee, B. K. (1982) *J. Virol.* **43,** 26–36.
25. Nagata, K., Satoh, T., Itoh, H., Kozasa, T., Okano, Y., Doi, T., Kaziro, Y. & Nozawa, Y. (1990) *FEBS Lett.* **275,** 29–32.
26. Novak, E. K., Sweet, H. O., Prochazka, M., Parentis, M., Soble, R., Reddington, M., Cairo, A. & Swank, R. T. (1988) *Br. J. Haematol.* **69,** 371–378.
27. Crosti, P. F. & Lucchelli, P. E. (1962) *J. Clin. Pathol.* **15,** 191–193.
28. Hui, S. W. & Costa, J. L. (1979) *J. Microsc.* **115,** 203–206.
29. Sviderskaya, E. V., Wakeling, W. F. & Bennett, D. C. (1995) *Development (Cambridge, U.K.)* **121,** 1547–1557.
30. Chen, D., Guo, J., Miki, T., Tachibana, M. & Gahl, W. A. (1997) *Biochem. Mol. Med.* **60,** 27–37.
31. Martinez, O. & Goud, B. (1998) *Biochim. Biophys. Acta* **1404,** 101–112.
32. Tolmachova, T., Ramalho, J. S., Anant, J. S., Schultz, R. A., Huxley, C. M. & Seabra, M. C. (1999) *Gene* **239,** 109–116.
33. Lane, P. W. & Womack, J. E. (1979) *J. Hered.* **70,** 133–135.

34. Langdon, W. Y., Theodore, T. S., Buckler, C. E., Stimpfling, J. H., Martin, M. A. & Morse, H. C. d. (1984) *Virology* **133,** 183–190.
35. Spritz, R. A. (1999) *Trends Genet.* **15,** 337–340.
36. Israels, S. J., McMillan, E. M., Robertson, C., Singhory, S. & McNicol, A. (1996) *Thromb. Haemost.* **75,** 623–629.
37. Dell'Angelica, E. C., Shotelersuk, V., Aguilar, R. C., Gahl, W. A. & Bonifacino, J. S. (1999) *Mol. Cell* **3,** 11–21.
38. Oh, J., Bailin, T., Fukai, K., Feng, G. H., Ho, L., Mao, J. I., Frenk, E., Tamura, N. & Spritz, R. A. (1996) *Nat. Genet.* **14,** 300–306.
39. Feng, G. H., Bailin, T., Oh, J. & Spritz, R. A. (1997) *Hum. Mol. Genet.* **6,** 793–797.
40. Gardner, J. M., Wildenberg, S. C., Keiper, N. M., Novak, E. K., Rusiniak, M. E., Swank, R. T., Puri, N., Finger, J. N., Hagiwara, N., Lehman, A. L., *et al.* (1997) *Proc. Natl. Acad. Sci. USA* **94,** 9238–9243.
41. Feng, L., Seymour, A. B., Jiang, S., To, A., Peden, A. A., Novak, E. K., Zhen, L., Rusiniak, M. E., Eicher, E. M., Robinson, M. S., *et al.* (1999) *Hum. Mol. Genet.* **8,** 323–330.
42. Andres, D. A., Seabra, M. C., Brown, M. S., Armstrong, S. A., Smeland, T. E., Cremers, F. P. & Goldstein, J. L. (1993) *Cell* **73,** 1091–1099.
43. Seabra, M. C., Ho, Y. K. & Anant, J. S. (1995) *J. Biol. Chem.* **270,** 24420–24427.
44. van den Hurk, J. A., Hendriks, W., van de Pol, D. J., Oerlemans, F., Jaissle, G., Ruther, K., Kohler, K., Hartmann, J., Zrenner, E., van Bokhoven, H., *et al.* (1997) *Hum. Mol. Genet.* **6,** 851–858.
45. Wei, Q., Wu, X. & Hammer, J. A., 3rd (1997) *J. Muscle Res. Cell Motil.* **18,** 517–527.
46. Wu, X., Bowers, B., Rao, K., Wei, Q. & Hammer, J. A. (1998) *J. Cell Biol.* **143,** 1899–1918.
47. Salminen, A. & Novick, P. J. (1987) *Cell* **49,** 527–538.
48. Johnston, G. C., Prendergast, J. A. & Singer, R. A. (1991) *J. Cell Biol.* **113,** 539–551.
49. Govindan, B., Bowser, R. & Novick, P. (1995) *J. Cell Biol.* **128,** 1055–1068.
50. Echard, A., Jollivet, F., Martinez, O., Lacapere, J. J., Rousselet, A., Janoueix-Lerosey, I. & Goud, B. (1998) *Science* **279,** 580–585.